AMERICAN ACADEMY OF OPHTHALMOLOGY®
In partnership with the AMERICAN GLAUCOMA SOCIETY

Comparison between Lamina Cribrosa Depth and Curvature as a Predictor of Progressive Retinal Nerve Fiber Layer Thinning in Primary Open-Angle Glaucoma

Eun Ji Lee, MD,[1] *Tae-Woo Kim, MD,*[1] *Hyunjoong Kim, PhD,*[2] *Seung Hyen Lee, MD,*[3] *Michaël J.A. Girard, PhD,*[4,5] *Jean Martial Mari, PhD*[6]

Purpose: To compare the ability of lamina cribrosa (LC) depth (LCD) and LC curvature to predict the rate of progressive retinal nerve fiber layer (RNFL) thinning in patients with primary open-angle glaucoma (POAG).

Design: Observational case series.

Participants: A total of 114 eyes of 114 patients diagnosed with POAG, in which RNFL thickness had been measured by serial spectral-domain (SD) OCT for at least 2.5 years.

Methods: The optic nerves of all participants underwent enhanced depth imaging volume scanning, and their circumpapillary RNFL thickness was measured using SD OCT, followed by regular serial measurements of RNFL thickness at intervals of ≥6 months. The LCD from the levels of Bruch's membrane (BM, LCD-BM) and the anterior sclera (AS, LCD-AS), and LC curvature index (LCCI) were measured by SD OCT at 3 locations: superior midperipheral, midhorizontal, and inferior midperipheral. The rate of RNFL thinning over time was determined by linear regression of serial OCT measurements of RNFL thickness.

Main Outcome Measures: Factors associated with the rate of OCT RNFL thinning.

Results: Univariate analysis showed that larger LCD-BM ($P = 0.001$), LCD-AS ($P < 0.001$), and LCCI ($P < 0.001$) were all significantly associated with a faster rate of global RNFL thinning. The LCCI showed a stronger correlation with the rate of global RNFL thinning than LCD-BM ($P < 0.001$) or LCD-AS ($P < 0.001$). Of the 3 variables, only LCCI remained significant on multivariate analysis ($P < 0.001$). Disc hemorrhage during follow-up ($P = 0.003$), wider parapapillary atrophy β-zone ($P = 0.017$), and greater global RNFL thickness ($P = 0.040$) were also significantly associated with a faster rate of global RNFL thinning.

Conclusions: Morphology of LC was significantly associated with the rate of progressive RNFL thinning. Curvature of LC better predicted progressive RNFL thinning than did LCD measured from the BM or AS. *Ophthalmology Glaucoma 2018;1:44-51 © 2018 by the American Academy of Ophthalmology*

Supplemental videos available at www.ophthalmologyglaucoma.org.

Posterior deformation of the lamina cribrosa (LC) is the principal event that induces axonal damage in glaucoma.[1-4] The LC deformation is thought to induce the death of retinal ganglion cells through various mechanisms, including blockade of axoplasmic flow and tissue remodeling by reactive astrocytes.[5-9] Recent experimental studies have shown that LC displacement occurs before detectable optic nerve damage.[2-4] The involvement of LC deformation and its occurrence before axonal damage in glaucomatous optic neuropathy suggest that LC morphology may predict disease outcomes.

Morphology of LC may be analyzed by various parameters. For example, LC depth (LCD) measured from the Bruch's membrane (BM) opening (LCD-BM) has been found to depend on intraocular pressure (IOP),[10,11] suggesting that LCD may be an indicator of IOP-related LC strain in glaucomatous eyes. Moreover, the LCD-BM was shown to be significantly associated with the rate of progressive retinal nerve fiber layer (RNFL) thinning in patients with primary open-angle glaucoma (POAG).[12] However, LCD-BM measurements include choroidal thickness, which varies among individuals.[13] Therefore, LCD-BM may provide an inaccurate assessment of LC strain. Recently, Vianna et al[14] suggested the anterior scleral (AS) opening as a more reliable reference structure to measure the LC position. The LCD measured from the AS opening (LCD-AS) may be more robust than LCD-BM because it is not influenced by the choroidal thickness.

Our group showed that the curvature of the LC, as assessed by the LC curvature index (LCCI), also may be a reliable parameter for evaluating LC morphology. We demonstrated that changes in LC curvature correlated with changes in IOP.[15] In addition, the LCCI performed better than LCD-BM in distinguishing between healthy and

https://doi.org/10.1016/j.ogla.2018.05.007
ISSN 2589-4196/18

glaucomatous eyes,[16] suggesting that LC curvature may better characterize LC deformation in glaucomatous eyes. More recently, we reported that the LCCI was associated with the rate of progressive RNFL thinning in glaucoma suspect eyes.[17]

Although several parameters have been described to assess LC strain, their relative accuracy and correlation with disease progression have not been determined. The present study compared the degree of association of LCD-BM, LCD-AS, and LCCI with the rate of progressive RNFL thinning in patients with primary open-angle glaucoma (POAG).

Methods

This investigation was a retrospective analysis of the data gathered from the Investigating Glaucoma Progression Study (IGPS), which is an ongoing prospective study of glaucoma patients at the Seoul National University Bundang Hospital Glaucoma Clinic, Seoul, South Korea. The study included consecutive subjects who met the eligibility criteria, all of whom provided written informed consent to participate. This study was approved by the Seoul National University Bundang Hospital Institutional Review Board and followed the tenets of the Declaration of Helsinki.

Study Subjects

Subjects who were enrolled in the IGPS underwent a comprehensive ophthalmic examination, including visual acuity assessment, Goldmann applanation tonometry, refraction tests, slit-lamp biomicroscopy, gonioscopy, dilated stereoscopic examination of the optic disc, disc photography (EOS D60 digital camera; Canon, Utsunomiyashi, Tochigiken, Japan), circumpapillary RNFL scanning, optic disc scanning (Spectralis; Heidelberg Engineering, Heidelberg, Germany), standard automated perimetry (Humphrey Field Analyzer II 750; 24-2 Swedish interactive threshold algorithm; Carl Zeiss Meditec, Dublin, CA), and measurements of corneal curvature (KR-1800; Topcon, Tokyo, Japan), central corneal thickness (Orbscan II; Bausch & Lomb Surgical, Rochester, NY), and axial length (IOL Master version 5; Carl Zeiss Meditec).

The IGPS excluded subjects with a history of intraocular surgery other than cataract extraction and glaucoma surgery, an intraocular disease (e.g., diabetic retinopathy or retinal vein occlusion) or a neurologic disease (e.g., pituitary tumor) that could cause visual field loss, and visual acuities worse than 20/40. All patients included in the IGPS were followed up every 3 to 6 months with regular follow-up fundus photography and spectral-domain (SD) OCT RNFL thickness was measured at intervals ranging from 6 months to 1 year. Patients included in the present study were required to be newly diagnosed with POAG, to have been followed up for at least 2.5 years with treatment, and to have undergone at least 5 serial OCT measurements. Primary open-angle glaucoma was defined as the presence of glaucomatous optic nerve damage (e.g., the presence of focal thinning, notching, and an RNFL defect), an associated glaucomatous visual field defect, and an open angle, as revealed by gonioscopy. A glaucomatous visual field defect was defined as (1) values outside the normal limits on the glaucoma hemifield test; (2) 3 abnormal points, with a probability of being normal of $P < 0.05$, and 1 point with a pattern deviation of $P < 0.01$; or (3) a pattern standard deviation of $P < 0.05$. Those visual field defects were confirmed on 2 consecutive reliable tests (fixation loss rate, ≤20%; false-positive and false-negative error rates, ≤25%).

Eyes with optic disc torsion of more than 15°[18] or a tilt ratio (minimum-to-maximum optic disc diameter) less than 0.75[19] and eyes with any abnormalities (including a large parapapillary atrophy [PPA]) in the circumpapillary region that affected the scan ring where the OCT RNFL thickness measurements were obtained were excluded from this study. A history of cataract surgery before the baseline examination was not an exclusion criterion in this study, but patients who underwent cataract surgery during the study were excluded because cataract extraction affects the signal quality of OCT scans and thus may influence the RNFL thickness data. Patients who underwent IOP-lowering surgery before or during the study also were excluded because the LC configuration may change substantially when the IOP re-elevates.[10,12]

Eyes also were excluded when a good-quality image (i.e., quality score >15) could not be obtained at more than 5 sections of enhanced depth imaging SD OCT disc scans (when the quality score does not reach 15, the image acquisition process automatically stops, and the image of the respective sections is not obtained). In addition, eyes were excluded when the images did not allow clear delineation of both the anterior and posterior borders of the central portion of the LC.

Untreated IOP was defined as the mean of at least 2 measurements before IOP-lowering treatment. The amount of IOP reduction was determined by calculating the percentage reduction of IOP at the final follow-up compared with the pretreatment level. The mean follow-up IOP measurement was obtained by averaging the IOP measured at 6-month intervals, and IOP fluctuation was determined using the standard deviation of these values.

A disc hemorrhage (DH) was defined as an isolated hemorrhage seen on the disc tissue or in the peripapillary retina connected to the disc rim.[20] A DH was detected by slit-lamp examination using a 78-diopter lens or a fundus photograph. Either of these was performed at every follow-up visit.

Enhanced Depth Imaging OCT of the Optic Disc

The optic nerve head (ONH) of each eye was imaged by Spectralis OCT using the enhanced depth imaging technique. The details and advantages of this technology for evaluating the LC have been described previously.[21,22]

Imaging was performed using a 10°×15° rectangle covering the optic disc. This rectangle was scanned with approximately 70 sections, which were 30 to 34 μm apart (the slicing distance is determined automatically by the machine). The average number of frames per section was 42, which provided the best trade-off between image quality and patient cooperation.[22] To enhance the visibility of the peripheral LC, all images were postprocessed using adaptive compensation.[23,24]

Measurements of Lamina Cribrosa Depth and Lamina Cribrosa Curvature Index

The LCDs and LCCIs on horizontal B-scan images were measured at 7 locations equidistant across the vertical optic disc diameter. These 7 B-scan lines, from the superior to the inferior regions, were defined as planes 1−7, respectively (Fig 1). In this model, plane 4 corresponds to the midhorizontal plane, and planes 2 and 6 correspond approximately to the superior and inferior midperiphery, respectively.

The LCD was measured both from the BM (LCD-BM) and the AS (LCD-AS). The reference planes of the BM and AS were determined on the basis of the peripheral BM,[14] which was defined as the location 800 μm from the BM opening (Fig 1). These reference points were chosen rather than the BM or AS opening, because the BM opening has been reported to migrate

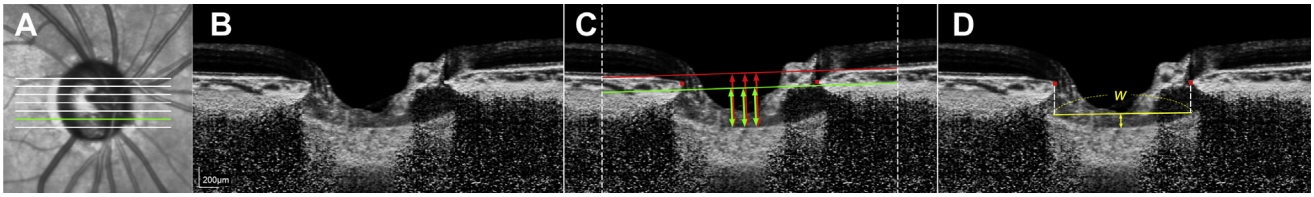

Figure 1. Measurements of lamina cribrosa (LC) deformation. **A,** Infrared image of an optic nerve head (ONH) showing the 7 locations at which the measurements were performed (*horizontal lines*). **B,** Enhanced depth image of plane 6 (**A,** *light green line*) processed by adaptive compensation. **C,** The same image as in **(B)**, showing the measurement of LC depth (LCD) from Bruch's membrane (LCD-BM, *red double headed arrows*) and from the anterior sclera (LCD-AS, *light green double-headed arrows*). *Red* and *light green lines* indicate the BM and AS reference planes, respectively, which were determined 800 μm (*dashed lines*) from the BM termination point (*red glyphs*). **D,** The same image as in **(B)**, showing the determination of LC curvature index (LCCI), which was measured by dividing the LC curve depth (*double headed arrow*) within the BM opening (*red glyphs* and *dashed lines*) by the BM opening width (*W*) and then multiplying by 100.

posteriorly with age[25] and acute[26] and chronic[27] IOP elevation, as well as to avoid irregularities and difficult visualizations that can occur in regions closer to the ONH.[14] The LCD-BM and LCD-AS were measured in the direction perpendicular to the BM and AS reference planes, respectively, at the maximally depressed points (Fig 1).

To quantify the posterior bowing of the LC on the B-scan images, the LCCI was defined as the inflection of a curve representing a section of the LC.[15,16] To measure the LCCI, a new reference line (LC surface reference line) was drawn on each B-scan by connecting the 2 points on the anterior LC surface that met the lines drawn from each BM termination point perpendicular to the reference line for the BM opening. The length of this reference line was defined as width (*W*), and the LC curve depth as the maximum depth from this reference line to the anterior LC surface (Fig 1). The LCCI was calculated as (LC curve depth/*W*) × 100. Because the curvature was normalized to the LC width, it describes the shape of the LC independent of the actual size of the ONH. Only the LC within the BM opening was considered, because the LC was often not clearly visible outside this opening.

Parameters at 7 points of the LC were measured using the manual caliper tool of the image processing software (Amira 5.2.2; Visage Imaging, Berlin, Germany) by 2 glaucoma specialists (EJL and SHL) who were blinded to clinical information. In eyes with LC defects, the LCD and LCCI were measured using a presumed anterior LC surface that best fit the curvature of the remaining part of the LC or excluding the area of the LC defect.

The LCD and LCCI were calculated by each observer, and the mean values determined by the 2 observers were averaged and analyzed. The measurements obtained from the 7 B-scans were used to calculate the mean LCD and the mean LCCI of the eye. The superior and inferior LCDs and LCCIs were defined as the means of the values obtained in planes 1 and 2, and planes 6 and 7, respectively.

Determination of the Parapapillary Atrophy Width

The PPA width was measured on enhanced depth imaging SD-OCT optic disc scans, as described previously.[28] On the basis of previous reports that the clinical characteristics and the rate of OCT RNFL thinning differ according to the extent of the BM within the PPA area,[28,29] the PPA was divided into β- and γ-zones, defined as areas with and without BM, respectively. The distances from the disc margin to the boundary of BM termination and from the BM termination to the PPA margin were defined as γ- and β-zone widths, respectively. Measurements were obtained from 3 of the 5 horizontal meridians, equally spaced within the vertical diameter of the optic disc, and the means of the measured values were analyzed.[28,29]

The PPA size was measured by a single observer (E.J.L.) blinded to each subject's clinical information. Excellent interobserver reproducibility for the measurement of PPA widths was reported previously.[28] A potential magnification error was removed by entering the corneal curvature of each eye into the Spectralis OCT system before SD OCT scanning.

Data Analysis

The interobserver reproducibility of LCD-BM, LCD-AS, and LCCI measurements was calculated using the intraclass correlation coefficients and 95% confidence intervals (CIs). The rate of change of RNFL thickness, expressed in micrometers per year, was determined by linear regression analysis. The associations of LCD-BM, LCD-AS, LCCI, and other factors with the rate of RNFL thinning were assessed by univariate analysis, with variables having a $P < 0.10$ entered into multivariate analysis.

All statistical analyses were performed using SPSS software version 20.0 (SPSS, Inc., Chicago, IL). Unless stated otherwise, the data are presented as mean ± standard deviation, with $P < 0.05$ considered statistically significant.

Results

Baseline Characteristics

The study initially enrolled 120 eyes of 120 patients with POAG who met the eligibility criteria. Six of these patients were excluded because of poor image quality that prevented the clear visualization of the anterior LC surface in at least 2 of the 7 B-scan images, leaving a final sample of 114 patients. Their mean ± standard deviation LCD-BM, LCD-AS, and LCCI were 520.1±100.8 μm (range, 268.8−777.8 μm), 440.4±83.4 μm (range, 225.6−648.0 μm), and 9.6±2.9 μm (range, 3.0−18.4 μm), respectively. The interobserver intraclass correlation coefficients for LCD-BM, LCD-AS, and LCCI measurements were 0.992 (95% CI, 0.988−0.994), 0.989 (95% CI, 0.984−0.992), and 0.988 (95% CI, 0.983−0.992), respectively. Table 1 summarizes the clinical characteristics of these patients.

Determination of Factors Associated with the Rate of Global Retinal Nerve Fiber Layer Thinning

Univariate analysis revealed that factors significantly associated with a faster rate of global RNFL thinning included DH during follow-up, larger PPA β-zone width, smaller PPA γ-zone width,

Table 1. Patient Clinical Characteristics

Age (yrs)	56.6±12.7 (22–82)
Gender (male/female)	53/61
Untreated IOP (mmHg)	15.7±4.1 (10–44)
IOP at SD OCT disc scanning (mmHg)	12.0±2.2 (8–18)
IOP at final FU (mmHg)	11.6±2.4 (6–19)
IOP reduction at final FU (%)	23.4±18.2 (−23.8 to 72.7)
IOP fluctuation during the FU (standard deviation)	1.5±0.6 (0.0–4.2)
Mean IOP during the FU (mmHg)	11.8±1.6 (8.4–17.4)
Refractive error (D)	−2.0±3.1 (−8.0 to 3.0)
Axial length (mm)	24.56±1.54 (21.60–29.51)
Central corneal thickness (μm)	556.6±31.9 (465–629)
Disc hemorrhage detection (%)	34.2 (39/114)
Baseline width of PPA β-zone (μm)	275.0±219.6 (0–848)
Baseline width of PPA γ-zone (μm)	150.6±259.5 (0–1496)
Visual field MD (dB)	−6.93±6.86 (−27.73 to 2.02)
Visual field PSD (dB)	7.47±4.86 (1.22–17.00)
Global RNFL thickness (μm)	73.4±14.4 (40–115)
Mean LCD-BM (μm)	520.1±100.8 (268.8–777.8)
Mean LCD-AS (μm)	440.4±83.4 (225.6–648.0)
Mean LCCI (μm)	9.6±2.9 (3.0–18.4)
Rate of global RNFL thinning (μm/yr)	−1.04±0.99 (−4.01 to 0.79)
FU period (yrs)	4.9±0.8 (2.5–8.6)
Number of SD OCT RNFL scans	7.6±1.4 (5–14)

Data are presented as mean ± standard deviation (range).
D = diopters; dB = decibels; FU = follow-up; IOP = intraocular pressure; LCCI = lamina cribrosa curvature index; LCD = lamina cribrosa depth; LCD-AS = LCD measured from anterior sclera; LCD-BM = LCD measured from Bruch's membrane; MD = mean deviation; PPA = parapapillary atrophy; PSD = pattern standard deviation; RNFL = retinal nerve fiber layer; SD = spectral-domain.

larger global RNFL thickness, greater visual field MD, and greater LCD-BM, LCD-AS, and LCCI. Multivariate analysis showed that the rate of global RNFL thinning was influenced significantly by LCCI, DH during follow-up, PPA β-zone width, and global RNFL thickness (Table 2).

Relationships between Regional Rate of Retinal Nerve Fiber Layer Thinning and Degree of Lamina Cribrosa Deformation

The LCD-BM ($R^2 = 0.096$, $P = 0.001$; Fig 2A), LCD-AS ($R^2 = 0.122$, $P < 0.001$; Fig 2B), and LCCI ($R^2 = 0.346$, $P < 0.001$; Fig 2C) all showed significant negative linear correlations with the rate of global RNFL thinning. Of these, LCCI showed a stronger correlation with the rate of global RNFL thinning than did LCD-BM ($P < 0.001$) or LCD-AS ($P < 0.001$).

In the superior region, LCD-AS ($R^2 = 0.061$, $P = 0.008$; Fig 2E) and LCCI ($R^2 = 0.308$, $P < 0.001$; Fig 2F) were significantly associated with the rate of RNFL thinning in the temporal-superior sector, with LCCI showing a stronger correlation than LCD-AS ($P < 0.001$). In contrast, LCD-BM was not significantly associated with the rate of RNFL thinning in this region ($R^2 = 0.026$, $P = 0.084$; Fig 2D).

In the inferior region, LCD-BM ($R^2 = 0.076$, $P = 0.003$; Fig 2G), LCD-AS ($R^2 = 0.069$, $P = 0.005$; Fig 2H), and LCCI ($R^2 = 0.122$, $P < 0.001$; Fig 2I) were significantly associated with the rate of RNFL thinning in the temporal-inferior sector. There were no statistically significant differences among these linear correlations.

Table 2. Factors Associated with Rate of Global Retinal Nerve Fiber Layer Thinning

	Univariate			Multivariate		
	Beta	*95% CI*	P *Value*	*Beta*	*95% CI*	P *Value*
Age, per 1 yr older	−0.002	−0.017 to 0.012	0.767			
Female gender	0.005	−0.365 to 0.374	0.980			
Untreated IOP, per 1 mmHg higher	−0.18	−0.064 to 0.027	0.422			
IOP at SD OCT disc scanning, per 1 mmHg higher	0.018	−0.066 to 0.101	0.672			
IOP at final FU, per 1 mmHg higher	−0.020	−0.098 to 0.058	0.610			
% IOP reduction at final FU, per 1% larger	0.002	−0.008 to 0.012	0.715			
IOP fluctuation during FU, per 1 mmHg larger	0.009	−0.301 to 0.319	0.955			
Mean IOP during FU, per 1 mmHg higher	0.015	−0.101 to 0.132	0.794			
Axial length, per 1 mm longer	0.043	−0.081 to 0.166	0.495			
Central corneal thickness, per 1 μm thicker	0.000	−0.006 to 0.006	0.952			
Disc hemorrhage	**−0.562**	**−0.936 to −0.188**	**0.004**	**−0.452**	**−0.742, −0.162**	**0.003**
Baseline width of PPA β-zone, per 10 μm larger	**−0.015**	**−0.022 to −0.007**	**<0.001**	**−0.008**	**−0.014, −0.001**	**0.017**
Baseline width of PPA γ-zone, per 10 μm larger	0.009	0.002 to 0.016	0.014	−0.001	−0.007, 0.005	0.722
Visual field MD, per 1 dB higher	−0.029	−0.055 to −0.002	0.033	−0.006	−0.035, 0.024	0.697
Visual field PSD, per 1 dB higher	0.024	−0.014 to 0.062	0.206			
Global RNFL thickness, per 1 μm thicker	**−0.021**	**−0.033 to −0.009**	**0.001**	**−0.015**	**−0.029, −0.001**	**0.040**
Mean LCD-BM, per 100 μm larger	**−0.304**	**−0.479 to −0.130**	**0.001**	−0.077	−0.397, 0.242	0.632
Mean LCD-AS, per 100 μm larger	**−0.414**	**−0.622 to −0.206**	**<0.001**	0.097	−0.316, 0.510	0.643
Mean LCCI, per 1 μm larger	**−0.202**	**−0.254 to −0.150**	**<0.001**	**−0.179**	**−0.245, −0.114**	**<0.001**
FU period, per 1 yr longer	0.057	−0.164 to 0.277	0.611			
No. of SD OCT RNFL scans, per 1 more scan	−0.051	−0.183 to 0.080	0.440			

Factors with statistical significance are shown in bold.
CI = confidence interval; dB = decibels; FU = follow-up; IOP = intraocular pressure; LCCI = lamina cribrosa curvature index; LCD = lamina cribrosa depth; LCD-AS = LCD measured from anterior sclera; LCD-BM = LCD measured from Bruch's membrane; MD = mean deviation; PPA = parapapillary atrophy; PSD = pattern standard deviation; RNFL = retinal nerve fiber layer; SD = spectral-domain.

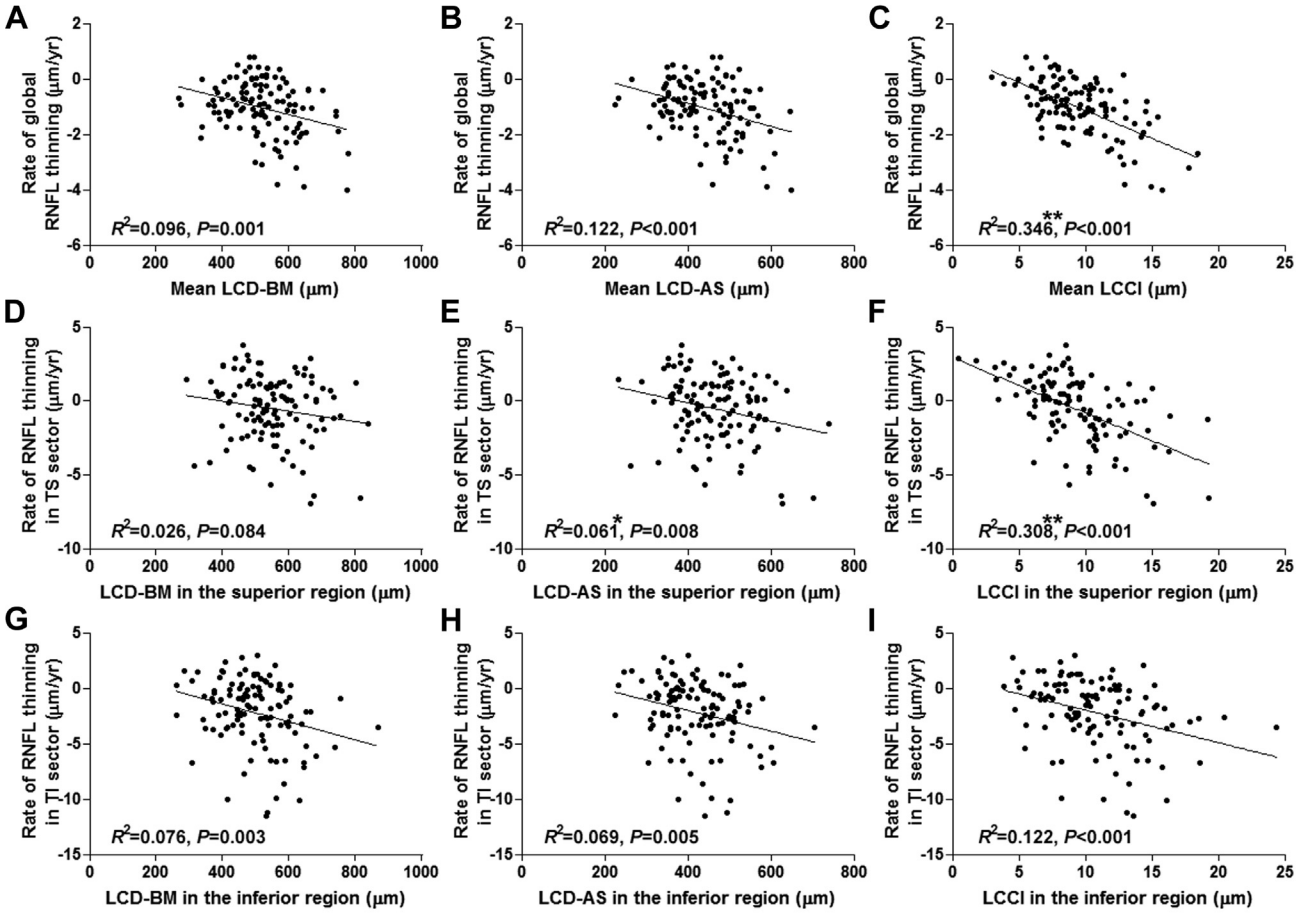

Figure 2. Scatterplots showing the relationships among the rates of global **(A–C)**, temporal-superior **(D–F)**, and temporal-inferior **(G–I)** retinal nerve fiber layer (RNFL) thinning and lamina cribrosa (LC) depth (LCD) from Bruch's membrane (BM) **(A, D, G)**, LCD anterior sclera (AS) **(B, E, H)**, and LCCI **(C, F, I)**. An asterisk indicates a significantly higher correlation than that of LCD-BM. Double asterisks indicate significantly higher correlations than those of both LCD-BM and LCD-AS. LCCI = lamina cribrosa curvature index; TI = temporal-inferior; TS = temporal-superior.

Representative Case

Figure 3 illustrates an eye with POAG that had a higher LCCI in the inferior than in the superior region. In contrast, neither LCD-BM nor LCD-AS shows noticeable inter-regional differences. Serial SD OCT examination showed that the rate of RNFL thinning was high in the temporal-inferior sector.

Discussion

In the present study, LC morphology in eyes with POAG was assessed by 3 different methods. Comparisons of these methods showed that the LCCI best predicted the rate of RNFL thinning, both globally and regionally, in both superior and inferior locations. This finding suggests that the LCCI may better represent the degree of LC strain than does LCD.

Currently available OCT devices can image the LC in the horizontal, vertical, and radial directions. In the present study, LC-related parameters were measured on horizontal B-scan images, because measuring the LCCI on vertical or radial scans is more complicated. The LC possesses a bowtie-shaped central ridge[30] and therefore often appears as a W-shape on vertical scans (Video 1, available at www.ophthalmologyglaucoma.org). This hampers the assessment of LC using a simple parameter such as the LCCI. In addition, the LC shape varies largely in radial scans along the meridians (Video 2, available at www.ophthalmologyglaucoma.org). In contrast, the LC shape is relatively uniform, with curvatures depending on the location of the scan (Video 3, available at www.ophthalmologyglaucoma.org).

Regional analysis showed that LCD-BM correlated only marginally with RNFL thinning, perhaps because the LCD-BM is affected by choroidal thickness, which is not associated with LC deformation. In contrast, LCD-AS is independent of choroidal thickness, suggesting that LCD-AS would show a closer association with progressive RNFL thinning than would LCD-BM.[14] However, its associations with the rates of global and temporal-inferior RNFL thinning were comparable to those of LCD-BM, except in the superior region, in which LCD-AS had only a slightly greater association with the rate of RNFL thinning than did LCD-BM. The reason why LCD-AS was not a better predictor of RNFL thinning rate than LCD-BM is unclear. The LCD-AS is influenced not only by posterior LC bowing but also by the level of LC insertion. The

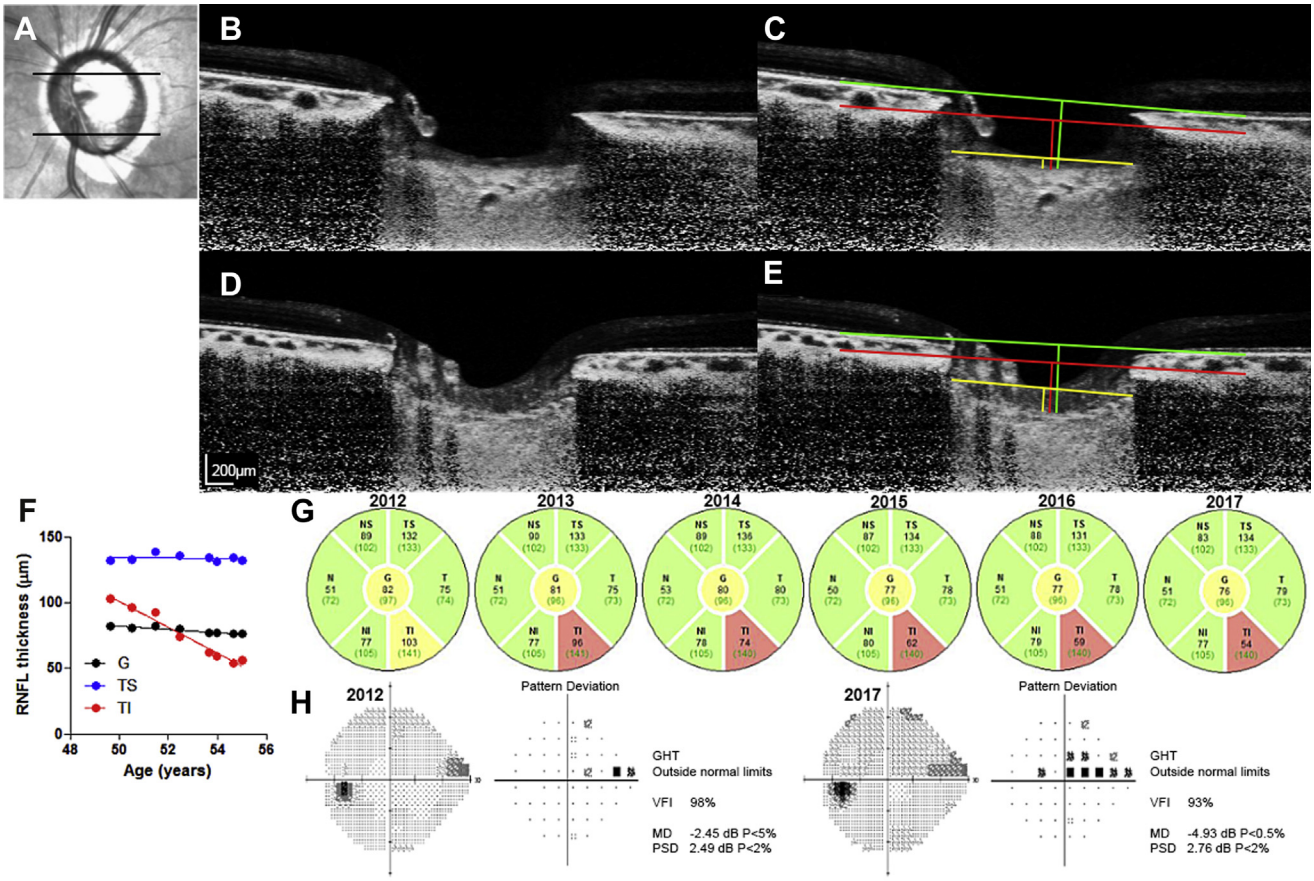

Figure 3. A glaucomatous eye showing progression at the location of greater lamina cribrosa (LC) curvature. **A,** Infrared image showing the locations at which the enhanced-depth images **(B–E)** were obtained. Enhanced-depth images in the superior **(B, C)** and inferior midperiphery **(D, E)** processed by adaptive compensation, showing greater LC curvature in the inferior **(E)** than in the superior **(C)** sector (*yellow lines*). In contrast, lamina cribrosa depth (LCD) measured from the level of Bruch's membrane (BM) (*green lines*) or the anterior sclera (AS) (*red lines*) does not differ noticeably between the inferior and superior regions. **F,** Note that the rate of retinal nerve fiber layer (RNFL) thinning is greater in the temporal-inferior (TI) than in the temporal-superior (TS) sector. **G,** Progressive RNFL thinning in the TI sector on serial OCT examination. **H,** Progressive visual field defect in the superior hemifield on standard automated perimetry. G = global; GHT = Glaucoma Hemifield Test; MD = mean deviation; PSD = pattern standard deviation; VFI = visual field index.

position of the LC insertion has been reported to migrate posteriorly as a result of active plastic remodeling of the tissue.[9,31,32] If posterior migration does not promote axonal damage, an eye with a large LCD-AS due to a large degree of posterior migration of LC insertion, but having a less bowed LC configuration, may not experience rapid glaucoma progression.

Our finding of progressive RNFL thinning in eyes with relatively smaller LCCI suggests that factors other than mechanical strain within the LC may play a role at least in some patients with POAG. Studies are needed to determine whether non–IOP-related factors, such as primary vascular dysregulation or low ocular perfusion pressure, are more frequent in this population.

The present study also found that none of the factors related to IOP was significantly associated with the rate of global RNFL thinning. This finding conflicts with previous results showing that IOP and its related parameters are important factors for glaucoma progression.[33-35] This discrepancy may be the result of the relatively low untreated (15.6±4.0 mmHg) and treated (12.0±1.5 mmHg) IOPs in our patients. In addition, eyes showing glaucoma progression received more intense IOP-lowering treatment, which may have led to a bias in the relationship between IOP parameters and the rate of RNFL thinning. Such a non-standardized treatment in patients in the IGPS also could have confounded the results of the associations between other baseline characteristics and the rate of RNFL thinning.

Together with larger LCCI, DH and a larger PPA β-zone area were significant independent predictors of more rapid global RNFL thinning, which is consistent with previous studies.[12,29,36-38] Thicker baseline RNFL was also found to be associated with the rate of RNFL thinning. This association may be related to the floor effect of the RNFL thickness. However, only 5 eyes had an RNFL thickness <50 µm in the present study. In addition, a subgroup analysis that excluded those 5 eyes still found a significant association of baseline RNFL thickness with the rate of RNFL thinning (data not presented). Therefore, this association cannot be simply explained by the floor effect. We consider that this is

more due to the absolute amount of reduced thickness being different according to the baseline RNFL thickness when the RNFL loss occurs in the same proportion (e.g., a 10% loss corresponds to 10-μm reduction for an eye with an RNFL thickness of 100 μm but 7 μm for an eye with an RNFL thickness of 70 μm). Because the rate of progression is calculated on the basis of the absolute RNFL thickness, the rate of RNFL thinning would be smaller in eyes with lower baseline RNFL thickness when the same proportion of existing axons disappears. The association of baseline RNFL thickness with the rate for RNFL thinning also has been found in previous studies.[12,29,39,40]

This study had several limitations. First, although precise quantification of LC curvature requires the LC surface reference line to be drawn from the LC insertion points, only the LC within the BM opening was included in the present study, because the LC was often not visible outside this region. However, we previously showed that in eyes in which the LC was visible up to the LC insertion, the LCCI measured from the entire LC (i.e., between the LC insertions) was comparable to that measured on the LC within the BM opening.[15] Thus, curvature of the LC assessed within the BM opening may be a surrogate for the actual LC curvature. In addition, we showed that LCCI was useful in diagnosing early glaucoma.[16] Second, a curvature is a geometric entity that refers specifically to the inverse of the radius of the arc of a circle that best fits the portion of a curve. Therefore, the LCCI does not correspond exactly to the actual LC curvature.

In conclusion, eyes with POAG and a larger degree of LC deformation exhibited a faster rate of RNFL thinning. The LCCI was a better predictor of future RNFL thinning than LCD-BM or LCD-AS, suggesting that LCCI better represents the mechanical strain within the LC than LCD and that LC curvature may be an important prognostic indicator of glaucoma progression.

References

1. Quigley HA, Addicks EM, Green WR, Maumenee AE. Optic nerve damage in human glaucoma. II. The site of injury and susceptibility to damage. *Arch Ophthalmol*. 1981;99:635–649.
2. Bellezza AJ, Rintalan CJ, Thompson HW, et al. Deformation of the lamina cribrosa and anterior scleral canal wall in early experimental glaucoma. *Invest Ophthalmol Vis Sci*. 2003;44:623–637.
3. Yang H, Downs JC, Bellezza A, et al. 3-D histomorphometry of the normal and early glaucomatous monkey optic nerve head: prelaminar neural tissues and cupping. *Invest Ophthalmol Vis Sci*. 2007;48:5068–5084.
4. Strouthidis NG, Fortune B, Yang H, et al. Longitudinal change detected by spectral domain optical coherence tomography in the optic nerve head and peripapillary retina in experimental glaucoma. *Invest Ophthalmol Vis Sci*. 2011;52:1206–1219.
5. Burgoyne CF, Downs JC, Bellezza AJ, et al. The optic nerve head as a biomechanical structure: a new paradigm for understanding the role of IOP-related stress and strain in the pathophysiology of glaucomatous optic nerve head damage. *Prog Retin Eye Res*. 2005;24:39–73.
6. Anderson DR, Hendrickson A. Effect of intraocular pressure on rapid axoplasmic transport in monkey optic nerve. *Invest Ophthalmol*. 1974;13:771–783.
7. Minckler DS, Bunt AH, Johanson GW. Orthograde and retrograde axoplasmic transport during acute ocular hypertension in the monkey. *Invest Ophthalmol Vis Sci*. 1977;16:426–441.
8. Minckler DS, Tso MO. A light microscopic, autoradiographic study of axoplasmic transport in the normal rhesus optic nerve head. *Am J Ophthalmol*. 1976;82:1–15.
9. Hernandez MR. The optic nerve head in glaucoma: role of astrocytes in tissue remodeling. *Prog Retin Eye Res*. 2000;19:297–321.
10. Lee EJ, Kim TW, Weinreb RN. Reversal of lamina cribrosa displacement and thickness after trabeculectomy in glaucoma. *Ophthalmology*. 2012;119:1359–1366.
11. Lee EJ, Kim TW, Weinreb RN. Variation of lamina cribrosa depth following trabeculectomy. *Invest Ophthalmol Vis Sci*. 2013;54:5392–5399.
12. Lee EJ, Kim TW, Kim M, Kim H. Influence of lamina cribrosa thickness and depth on the rate of progressive retinal nerve fiber layer thinning. *Ophthalmology*. 2015;122:721–729.
13. Rhodes LA, Huisingh C, Johnstone J, et al. Peripapillary choroidal thickness variation with age and race in normal eyes. *Invest Ophthalmol Vis Sci*. 2015;56:1872–1879.
14. Vianna JR, Lanoe VR, Quach J, et al. Serial changes in lamina cribrosa depth and neuroretinal parameters in glaucoma: impact of choroidal thickness. *Ophthalmology*. 2017;124:1392–1402.
15. Lee SH, Yu DA, Kim TW, et al. Reduction of the lamina cribrosa curvature after trabeculectomy in glaucoma. *Invest Ophthalmol Vis Sci*. 2016;57:5006–5014.
16. Lee SH, Kim TW, Lee EJ, et al. Diagnostic power of lamina cribrosa depth and curvature in glaucoma. *Invest Ophthalmol Vis Sci*. 2017;58:755–762.
17. Kim JA, Kim TW, Weinreb RN, et al. Lamina cribrosa morphology predicts progressive retinal nerve fiber layer loss in eyes with suspected glaucoma. *Sci Rep*. 2018;8:738.
18. Vongphanit J, Mitchell P, Wang JJ. Population prevalence of tilted optic disks and the relationship of this sign to refractive error. *Am J Ophthalmol*. 2002;133:679–685.
19. Jonas JB, Kling F, Grundler AE. Optic disc shape, corneal astigmatism, and amblyopia. *Ophthalmology*. 1997;104:1934–1937.
20. Gordon MO, Beiser JA, Brandt JD, et al. The Ocular Hypertension Treatment Study: baseline factors that predict the onset of primary open-angle glaucoma. *Arch Ophthalmol*. 2002;120:714–720. discussion 829-830.
21. Spaide RF, Koizumi H, Pozzoni MC. Enhanced depth imaging spectral-domain optical coherence tomography. *Am J Ophthalmol*. 2008;146:496–500.
22. Lee EJ, Kim TW, Weinreb RN, et al. Visualization of the lamina cribrosa using enhanced depth imaging spectral-domain optical coherence tomography. *Am J Ophthalmol*. 2011;152:87–95.e1.
23. Girard MJ, Strouthidis NG, Ethier CR, Mari JM. Shadow removal and contrast enhancement in optical coherence tomography images of the human optic nerve head. *Invest Ophthalmol Vis Sci*. 2011;52:7738–7748.
24. Mari JM, Strouthidis NG, Park SC, Girard MJ. Enhancement of lamina cribrosa visibility in optical coherence tomography images using adaptive compensation. *Invest Ophthalmol Vis Sci*. 2013;54:2238–2247.
25. Johnstone J, Fazio M, Rojananuangnit K, et al. Variation of the axial location of Bruch's membrane opening with age, choroidal thickness, and race. *Invest Ophthalmol Vis Sci*. 2014;55:2004–2009.

26. Strouthidis NG, Fortune B, Yang H, et al. Effect of acute intraocular pressure elevation on the monkey optic nerve head as detected by spectral domain optical coherence tomography. *Invest Ophthalmol Vis Sci*. 2011;52:9431−9437.
27. He L, Yang H, Gardiner SK, et al. Longitudinal detection of optic nerve head changes by spectral domain optical coherence tomography in early experimental glaucoma. *Invest Ophthalmol Vis Sci*. 2014;55:574−586.
28. Kim M, Kim TW, Weinreb RN, Lee EJ. Differentiation of parapapillary atrophy using spectral-domain optical coherence tomography. *Ophthalmology*. 2013;120:1790−1797.
29. Kim YW, Lee EJ, Kim TW, et al. Microstructure of beta-zone parapapillary atrophy and rate of retinal nerve fiber layer thinning in primary open-angle glaucoma. *Ophthalmology*. 2014;121:1341−1349.
30. Park SC, Kiumehr S, Teng CC, et al. Horizontal central ridge of the lamina cribrosa and regional differences in laminar insertion in healthy subjects. *Invest Ophthalmol Vis Sci*. 2012;53:1610−1616.
31. Yang H, Williams G, Downs JC, et al. Posterior (outward) migration of the lamina cribrosa and early cupping in monkey experimental glaucoma. *Invest Ophthalmol Vis Sci*. 2011;52:7109−7121.
32. Downs JC, Roberts MD, Burgoyne CF. Mechanical environment of the optic nerve head in glaucoma. *Optom Vis Sci*. 2008;85:425−435.
33. The effectiveness of intraocular pressure reduction in the treatment of normal-tension glaucoma. Collaborative Normal-Tension Glaucoma Study Group. *Am J Ophthalmol*. 1998;126:498−505.
34. The Advanced Glaucoma Intervention Study (AGIS): 7. The relationship between control of intraocular pressure and visual field deterioration. The AGIS Investigators. *Am J Ophthalmol*. 2000;130:429−440.
35. Leske MC, Heijl A, Hussein M, et al. Factors for glaucoma progression and the effect of treatment: the Early Manifest Glaucoma Trial. *Arch Ophthalmol*. 2003;121:48−56.
36. Kim KE, Jeoung JW, Kim DM, et al. Long-term follow-up in preperimetric open-angle glaucoma: progression rates and associated factors. *Am J Ophthalmol*. 2015;159:160−168.e1-2.
37. Faridi OS, Park SC, Kabadi R, et al. Effect of focal lamina cribrosa defect on glaucomatous visual field progression. *Ophthalmology*. 2014;121:1524−1530.
38. Yamada H, Akagi T, Nakanishi H, et al. Microstructure of peripapillary atrophy and subsequent visual field progression in treated primary open-angle glaucoma. *Ophthalmology*. 2016;123:542−551.
39. Leung CK, Cheung CY, Weinreb RN, et al. Evaluation of retinal nerve fiber layer progression in glaucoma: a study on optical coherence tomography guided progression analysis. *Invest Ophthalmol Vis Sci*. 2010;51:217−222.
40. Medeiros FA, Alencar LM, Zangwill LM, et al. Detection of progressive retinal nerve fiber layer loss in glaucoma using scanning laser polarimetry with variable corneal compensation. *Invest Ophthalmol Vis Sci*. 2009;50:1675−1681.

Footnotes and Financial Disclosures

Originally received: April 2, 2018.
Final revision: May 31, 2018.
Accepted: May 31, 2018.
Available online: June 29, 2018. Manuscript no. 2018-3.

[1] Department of Ophthalmology, Seoul National University Bundang Hospital, Seongnam, Korea.

[2] Department of Applied Statistics, Yonsei University, Seoul, Korea.

[3] Department of Ophthalmology, Bundang Jesaeng General Hospital, Daejin Medical Center, Seongnam, Korea.

[4] Department of Biomedical Engineering, National University of Singapore, Singapore.

[5] Singapore Eye Research Institute, Singapore National Eye Centre, Singapore.

[6] GePaSud, Université de la Polynésie Française, Tahiti, French Polynesia.

Financial Disclosure(s):
The author(s) have no proprietary or commercial interest in any materials discussed in this article.

Supported by the Seoul National University Bundang Hospital Research Fund (No. 02-2016-023) and Basic Science Research program through the National Research Foundation of Korea (NRF) funded by the Ministry of Education, Science, and Technology, Seoul, South Korea (No. 2016R1D1A1B02011696). The funder had no role in the design or conduct of this research.

HUMAN SUBJECTS: Human subjects were included in this study. The human ethics committees at the Seoul National University Bundang Hospital approved the study. All research adhered to the tenets of the Declaration of Helsinki. All participants provided informed consent.

No animal subjects were used in this study.

Author Contributions:

Conception and design: Lee, T-W. Kim

Data collection: Lee, T-W. Kim, Lee

Analysis and interpretation: Lee, T-W. Kim, H. Kim, Lee, Girard, Mari

Obtained funding: H. Kim

Overall responsibility: Lee, T-W. Kim, H. Kim, Lee, Girard, Mari

Abbreviations and Acronyms:
AS = anterior sclera; **BM** = Bruch's membrane; **CI** = confidence interval; **DH** = disc hemorrhage; **IGPS** = Investigating Glaucoma Progression Study; **IOP** = intraocular pressure; **LC** = lamina cribrosa; **LCCI** = lamina cribrosa curvature index; **LCD** = lamina cribrosa depth; **ONH** = optic nerve head; **POAG** = primary open-angle glaucoma; **PPA** = parapapillary atrophy; **RNFL** = retinal nerve fiber layer; **SD** = spectral-domain.

Correspondence:
Tae-Woo Kim, MD, Department of Ophthalmology, Seoul National University Bundang Hospital, Seoul National University College of Medicine 82, Gumi-ro, 173 Beon-gil, Bundang-gu, Seongnam, Gyeonggi-do 463-707, Korea. E-mail: twkim7@snu.ac.kr.